


## RESEARCH ARTICLE

# Cortical depth profiles of auditory and visual 7 T functional MRI responses in human superior temporal areas

Kaisu Lankinen<sup>1,2</sup>  | Seppo P. Ahlfors<sup>1,2</sup>  | Fahimeh Mamashli<sup>1,2</sup>  |  
 Anna I. Blazejewska<sup>1,2</sup> | Tommi Raji<sup>1,2</sup>  | Tori Turpin<sup>1</sup> |  
 Jonathan R. Polimeni<sup>1,2,3</sup>  | Jyrki Ahveninen<sup>1,2</sup> 

<sup>1</sup>Athinoula A. Martinos Center for Biomedical Imaging, Department of Radiology, Massachusetts General Hospital, Charlestown, Massachusetts, USA

<sup>2</sup>Department of Radiology, Harvard Medical School, Boston, Massachusetts, USA

<sup>3</sup>Division of Health Sciences and Technology, Massachusetts Institute of Technology, Cambridge, Massachusetts, USA

## Correspondence

Kaisu Lankinen, Athinoula A. Martinos Center for Biomedical Imaging, Department of Radiology, Massachusetts General Hospital, 149, 13th Street, Charlestown, MA 02129, USA.

Email: [klankinen@mgh.harvard.edu](mailto:klankinen@mgh.harvard.edu)

## Funding information

National Institutes of Health, Grant/Award Numbers: K99MH120054, P41EB015896, R01DC016765, R01DC016915, R01DC017991

## Abstract

Invasive neurophysiological studies in nonhuman primates have shown different laminar activation profiles to auditory vs. visual stimuli in auditory cortices and adjacent polymodal areas. Means to examine the underlying feedforward vs. feedback type influences noninvasively have been limited in humans. Here, using 1-mm isotropic resolution 3D echo-planar imaging at 7 T, we studied the intracortical depth profiles of functional magnetic resonance imaging (fMRI) blood oxygenation level dependent (BOLD) signals to brief auditory (noise bursts) and visual (checkerboard) stimuli. BOLD percent-signal-changes were estimated at 11 equally spaced intracortical depths, within regions-of-interest encompassing auditory (Heschl's gyrus, Heschl's sulcus, planum temporale, and posterior superior temporal gyrus) and polymodal (middle and posterior superior temporal sulcus) areas. Effects of differing BOLD signal strengths for auditory and visual stimuli were controlled via normalization and statistical modeling. The BOLD depth profile shapes, modeled with quadratic regression, were significantly different for auditory vs. visual stimuli in auditory cortices, but not in polymodal areas. The different depth profiles could reflect sensory-specific feedforward versus cross-sensory feedback influences, previously shown in laminar recordings in nonhuman primates. The results suggest that intracortical BOLD profiles can help distinguish between feedforward and feedback type influences in the human brain. Further experimental studies are still needed to clarify how underlying signal strength influences BOLD depth profiles under different stimulus conditions.

## KEYWORDS

cortical layers, feedforward/feedback, high-resolution fMRI

## 1 | INTRODUCTION

Neuroanatomical studies in nonhuman primates (NHP) have revealed a hierarchical organization among areas of the cerebral cortex, defined

by laminar distributions of the origins and terminations of the connections between areas (Felleman & Van Essen, 1991; Rockland & Pandya, 1979; Zeki, 2018). The inter-area connections are described as being of feedforward (FF), feedback (FB), or lateral type. Laminar

This is an open access article under the terms of the [Creative Commons Attribution-NonCommercial-NoDerivs](https://creativecommons.org/licenses/by-nc-nd/4.0/) License, which permits use and distribution in any medium, provided the original work is properly cited, the use is non-commercial and no modifications or adaptations are made.

© 2022 The Authors. *Human Brain Mapping* published by Wiley Periodicals LLC.

patterns corresponding to different types of inputs into cortical areas have been identified also functionally in NHPs using electrophysiological recordings, with FF inputs targeting the granular layer in the middle and FB inputs arriving above and below the granular layer (Lakatos et al., 2007, 2009; Schroeder et al., 2001; Schroeder & Foxe, 2002). Characterizing such FF and FB influences provides valuable information for understanding neural processing in the cerebral cortex (see, e.g., Walker & Hickok, 2016), and determining these noninvasively in humans is of considerable interest (Petro & Muckli, 2017; Yang et al., 2021).

Recent advances in functional magnetic resonance imaging (fMRI) have enabled imaging blood oxygenation level dependent (BOLD) signals with high enough spatial resolution ( $\leq 1 \text{ mm}^3$  voxel size) to study activation depth profiles across the cortical layers in humans (Finn et al., 2019; Norris & Polimeni, 2019; Polimeni et al., 2018). Several studies have used depth profiles of BOLD signals to dissociate different input types in the visual cortex (Fracasso et al., 2018; Klein et al., 2018; Kok et al., 2016; Lawrence et al., 2019; Muckli et al., 2015). BOLD depth profiles could be particularly well suited for the investigation of human auditory cortices (Ahveninen et al., 2016; De Martino et al., 2015; Moerel et al., 2018; Moerel et al., 2019; Wu et al., 2018), which are generally thicker than visual cortices (Fischl & Dale, 2000). Recent 7 T fMRI studies have examined depth profiles of also multisensory and attentional influences in auditory cortex (Gau et al., 2020) as well as columnar and laminar distribution of audiovisual processing of motion stimuli in planum temporale (PT) (Chai et al., 2021). In this study, we characterize the cortical depth profiles of BOLD signals in auditory and polymodal cortical areas in response to auditory and visual stimulation.

A well-established neurophysiological model of FF and FB influences in NHP provides specific predictions for depth profiles for our human study (Lakatos et al., 2009; Schroeder & Foxe, 2002). There is converging evidence that cross-sensory influences already take place in early auditory cortex, shown by both NHP neurophysiological studies (see, e.g., Foxe & Schroeder, 2005; Ghazanfar & Schroeder, 2006; Kayser & Logothetis, 2007; Schroeder & Foxe, 2005) and human neuroimaging studies (Beauchamp et al., 2004; Foxe et al., 2002; Kayser et al., 2005; Noesselt et al., 2007; Raji et al., 2000; Raji et al., 2010; Rohe & Noppeney, 2016). In NHP auditory cortices, cross-sensory inputs can be of FF or FB type, depending on the hierarchical level of the receiving auditory area and the sensory modality of the inputs (Lakatos et al., 2007, 2009; Schroeder et al., 2001; Schroeder & Foxe, 2002). In and near the primary auditory cortex, cross-sensory visual stimuli result in FB type laminar activation patterns (in superficial and deep layers), in contrast to the FF type patterns (middle layer) evoked by auditory input. In the NHP superior temporal polysensory (STP) area, the laminar profiles are of FF type for both auditory and visual stimulation (Schroeder & Foxe, 2002). We predicted that the cortical depth profiles of the BOLD signal in response to auditory vs. visual stimulation would be qualitatively different in the primary auditory cortex (corresponding to FF vs. FB type inputs), whereas in a polymodal superior temporal region, homologous to the STP in NHP, the depth profiles would be similar.

One of the challenges in the interpretation of depth-dependent fMRI is the BOLD signal from large veins, which bias the estimated activation toward the superficial pial surface (Markuerkiaga et al., 2016; Olman et al., 2007; Polimeni et al., 2010; Turner, 2002). In addition, intracortical radial ascending veins may affect the BOLD signal across the cortical layers (Markuerkiaga et al., 2016; van Dijk et al., 2020, 2021). The small voxel-size provided with high-field fMRI helps to reduce the partial-volume effect from pial matter (Blazejewska et al., 2019). We used  $1 \text{ mm}^3$  isotropic resolution 3D echo-planar imaging (EPI) at 7 T, which has been shown to provide better sensitivity and shorter volume acquisition time (although having larger vulnerability to physiological artifacts and movement) in visual cortex, compared with more conventional 2D-EPI, although depending of the protocol (Poser et al., 2010). For the depth profile analysis, we resampled the fMRI data into 11 equally spaced surfaces within the cortical gray matter, and compared the different task conditions (auditory vs. visual) in the same vertices across the gray matter. Previous studies have demonstrated that the BOLD signal increases from deep to superficial layers (e.g., Chai et al., 2021; Gau et al., 2020; Markuerkiaga et al., 2016; Polimeni et al., 2010). We described the shape of the activation depth profiles by fitting a quadratic polynomial to the BOLD %-signal-change profile. The quadratic model enabled us to investigate nonlinear depth dependence. A concave (“inverted-U”) shape, indicating larger BOLD signal in the middle cortical layers relative to a linear profile, could potentially correspond to the distribution of FF type inputs, whereas a convex shape, indicating relatively larger BOLD signal in the lower and upper layers, could correspond to FB type inputs. Using these approaches, we demonstrate distinct depth profiles of cortical activation in response to auditory and visual stimulation in primary auditory versus adjacent polymodal areas.

## 2 | MATERIALS AND METHODS

### 2.1 | Participants

Thirteen right-handed adults (8 females, 23–35 years) with no neurological disorders or psychiatric conditions participated. Potential subjects were first screened to ensure that they are MRI compatible and that they had normal hearing and vision. The study protocol was approved by the Institutional Review Board at Massachusetts General Hospital. The subjects gave written informed consent prior to the experiments.

### 2.2 | Task and stimuli

Subjects were presented 300-ms auditory (A), visual (V), and audiovisual (AV; simultaneous auditory and visual) stimuli (Raji et al., 2010). One run consisted of 45 stimuli in trains of 5 stimuli of the same category. The trains were presented in pseudorandom order with a 6-s interval between them; the stimulus onset asynchrony between the

stimuli within a train was 1.5 s. A, V, and AV stimuli were equiprobable. In 50% of the stimulus trains, one of the five stimulus events was a target event (*i.e.*, 10% of all events). The auditory stimuli were 300-ms Gaussian noise bursts filtered at 200–8000 Hz and with 10-ms onset and offset ramps. The visual stimuli were foveally presented checkerboard patterns, with visual angle  $3.5^\circ \times 3.5^\circ$  and contrast 100%. The audiovisual stimuli were combinations of the A and V stimuli. The auditory target event was a 1000-Hz pure tone, the visual target a checkerboard pattern with a gray diamond-shaped pattern in the middle, and the AV target the combination of auditory and visual targets. The subjects were asked to press a button with the right-hand index finger as quickly as possible upon detecting a target. Two of the subjects had three runs, one had five runs, and the rest of the subjects had four runs per session. Seven of the 13 subjects had two sessions. For those subjects, the general linear model (GLM) was fit separately for both sessions, and the session was used as a variable in the linear mixed-effect (LME) model (see below).

### 2.3 | Data acquisition

7 Tesla MRI was obtained using a whole-body scanner (MAGNETOM, Siemens, Erlangen, Germany) with a 32-channel RF loop coil head array (Keil et al., 2010). Anatomical T<sub>1</sub> data were acquired using a 0.75 mm isotropic MEMPRAGE pulse sequence (van der Kouwe et al., 2008). For functional data acquisition with 1.0-mm isotropic resolution, we used a gradient-echo 3D-EPI protocol (WIP1080 prototype sequence from Siemens) with the following parameters: 44 partitions with thickness 1.0 mm positioned to optimize the coverage for superior temporal regions, TR/TE = 3.068 s/30 ms, flip angle 14°, no fat suppression, field of view = 192 × 192 mm<sup>2</sup>, 192 × 192 matrix, bandwidth = 1628 Hz/pixel, acceleration factor in phase encoding direction 4, acceleration factor in 3D direction 1, nominal echo spacing = 1 ms, and CAIPI shift  $k_z = 0$ ,  $k_y = 1$ . The images were reconstructed by using the GRAPPA pipeline (Griswold et al., 2002), as provided by the vendor. Head motion during the scans was minimized by firm support, and head motion was detected and corrected in the preprocessing. See Data S1 for an example of raw EPI data (Figure S1), and for temporal signal-to-noise ratio for a phantom and one representative subject, respectively (Figures S2 and S3).

### 2.4 | Analysis of anatomical MRI

Bias field correction, cortical surface reconstructions, coregistration of anatomical and functional data, as well as fMRI data-analyses were conducted using FreeSurfer 6.0 (Fischl, 2012) with an extension for submillimeter 7 T data (Zaretskaya et al., 2015) and our in-house software using Matlab 2019b (The MathWorks, Inc., Natick, Massachusetts, USA). Surface reconstructions of the interfaces between the cortical gray matter vs. the underlying white matter and pial surface were automatically generated from the anatomical MRI data (Fischl, 2012). Nine additional surfaces were created at fixed relative

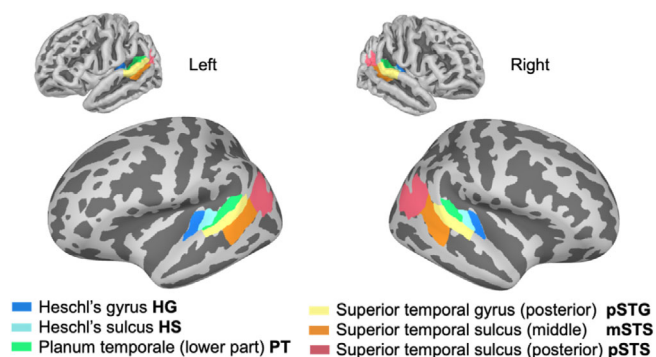


**FIGURE 1** Cortical regions-of-interest, based on Destrieux and Desikan-Killiany atlases, used in the depth profile analysis. The inflated surfaces of FreeSurfer's fsaverage template, shown rotated 25° around the vertical axis, are used here only for illustration purposes; all analyses were performed separately using individual subjects' data

distances between the white matter border and pial surfaces determined from the cortical thickness (Polimeni et al., 2010). Even though the number of surfaces is large compared with the functional resolution, it can still improve depth profile visualization and minimize partial volume effects between neighboring voxels (Huber et al., 2018). All surfaces created by FreeSurfer for an individual subject had the same number of vertices, allowing corresponding vertices in each of the 11 surfaces to be used for the depth profile analysis. An example of the gray and white matter surfaces overlaid on a cross-section of the anatomical data is shown in Figure S4.

We selected six cortical regions-of-interest (ROIs) in each hemisphere based on the Destrieux and Desikan-Killiany atlases provided by FreeSurfer (Desikan et al., 2006; Fischl et al., 2004; Figure 1). The ROIs were chosen to cover primary and nonprimary auditory regions and polymodal superior temporal regions: Heschl's gyrus (HG), Heschl's sulcus (HS), lower part of planum temporale (PT; masked with supramarginal area of the FreeSurfer Desikan-Killiany atlas), posterior part of superior temporal gyrus (pSTG), and middle and posterior parts of superior temporal sulcus (mSTS and pSTS).

### 2.5 | Preprocessing of fMRI data

Individual functional volumes were motion-corrected to the middle volume of each run, co-registered with each subject's structural MRI using Boundary-Based Registration (Greve & Fischl, 2009), and intensity normalized (see Figure S5 for coregistration of functional volumes to the anatomical surfaces). Since these 3D-EPI data were encoded in 3D, there were no slice timing differences and thus no slice-timing correction was applied. The fMRI time series were resampled onto the 11 surfaces by projecting each intersecting functional voxel onto the corresponding surface vertices using trilinear interpolation. See Figure S6 for example of surface BOLD signal time series and Figure S7 for functional signal-to-noise ratio. BOLD signal time series for each of the 11 surfaces were separately entered into a GLM with the task conditions (A, V, and AV) as

explanatory variables. Slow trends in the data were removed by high-pass filtering at 0.01 Hz. In addition, instead of a conventional volumetric approach, the data were smoothed along the surface using a 2D Gaussian kernel with 3 mm FWHM.

To select the vertices for the depth profile analysis within each ROI, we averaged the activity in the AV condition in the seven middle surfaces (excluding two surfaces from the top and two from the bottom) and selected the vertices with a significant positive value ( $p < .05$ , uncorrected). Thus, each surface had same number of vertices from which values were selected when comparing the A and V conditions, thereby controlling for potential layer sensitivity bias. For the A and V conditions, all positive %-signal-change values within each ROI were averaged, separately for each surface, from the set of vertices selected based on the AV condition. Figure S8 shows %-signal-changes (positive values) of conditions AV, A, and V in vertices used for calculating the depth profiles; all ROIs included significant vertices, but the exact number depended on the individual subject. Because of the inherent differences in the response strength between the conditions, the data were z-score normalized by subtracting the mean and dividing by the standard deviation of the data. This normalization was performed separately within each condition, ROI and hemisphere, but across subjects and surfaces (see Figure S9 for details).

## 2.6 | Depth profile analysis of fMRI data

The shape of the depth profiles of the BOLD signal was modeled as a quadratic polynomial:

$$z(x) = ax^2 + bx + c \quad (1)$$

where  $z(x)$  is the (normalized) %-signal-change value and  $x$  represents cortical depth corresponding to the 11 surfaces. In our analyses,  $x$  was centered around 0, with  $-5$  corresponding to the white matter border and  $+5$  the pial surface, thus making  $x$  and  $x^2$  fully orthogonal. Our main interest was in evaluating potential differences between the A and V conditions in the coefficient  $a$  for the second-order term. We focused on normalized data to control for the possibility that strong amplitude differences between auditory and visual conditions in certain ROIs might bias the estimated coefficient values of the statistical model. Results for nonnormalized data are presented in Data S1.

To evaluate task-related differences in the depth profiles, we used a linear mixed-effect model (fitlme provided by Matlab, 2019b) defined by the formula (Wilkinson notation; Wilkinson & Rogers, 1973):

$$\text{response} \sim 1 + \text{condition} + \text{surface} + \text{surface}^2 + \text{condition} : \text{surface} + \text{condition} : \text{surface}^2 + (1|\text{subject}) + (1|\text{subject} : \text{session}), \quad (2)$$

where *response* is the normalized %-signal-change value, 1 is the *intercept*, *condition* (A, V), *surface* and *surface*<sup>2</sup> are predictors, and *subject*

and *session* are grouping variables. Thus, the model has fixed effects for *intercept*, *condition*, *surface*, and *surface*<sup>2</sup> as well as their interactions, and random effects for *subject* and *session* within a subject. Here, we primarily focused on the interactions quantifying the task-related differences in the shape of the depth profile, i.e., the term *condition* by *surface*<sup>2</sup>. The LME model of Equation (1) can be written as:

$$z_{st}^r(m, x) = \beta_0^r + \beta_1^r m + (\beta_2^r + \beta_{12}^r m)x + (\beta_3^r + \beta_{13}^r m)x^2 + \eta_{0s}^r + \eta_{0st}^r + e_{st}^r(m, x), \quad (3)$$

where  $z$  is the (normalized) %-signal change;  $s$  and  $t$  are indices for subject and session, respectively;  $r$  is ROI (6 ROIs in each hemisphere);  $m$  is an indicator variable for the stimulus condition (the sensory modality, A, or V);  $x$  represents the cortical depth (the 11 surfaces);  $\beta$  are coefficients for fixed effects,  $\eta$  are coefficients for random effects and  $e$  is the error term. The significance threshold for testing two hemispheres, six ROIs, and six fixed effect terms was  $p < .05$ , with false discovery rate (FDR) correction for multiple comparisons. The resulting LME model was also used to estimate and visualize fitted (or “predicted”) depth profiles.

To describe the characteristics of the depth profiles with a simple measure, and to help visualize the shape parameters in a cortical surface representation, we also fitted a quadratic polynomial regression for each ROI and subject separately. We then evaluated differences between A and V separately for the quadratic, linear, and constant polynomial coefficients. The statistical significance of differences between A and V for these coefficients was determined using a *secondary* LME model

$$\text{poly} \sim 1 + \text{condition} + (1|\text{subject}) + (1|\text{subject} : \text{session}), \quad (4)$$

where *poly* is polynomial coefficient ( $a$ ,  $b$ , or  $c$  in Equation 1) from all subjects (response variable), 1 represents the *intercept*, *condition* (A, V) is the predictor, and *subject* and *session* are the grouping variables. Thus, the model had fixed effects for *intercept* and *condition*, and a random effect for *subject* and *session*. The significance threshold for testing two hemispheres, six ROIs, and three coefficients was  $p < .05$ , with FDR correction for multiple comparisons.

## 3 | RESULTS

### 3.1 | Depth profiles in A and V responses in and near auditory cortices

A summary of the BOLD signal depth profile analysis and results is provided in Figure 2. The fMRI data were resampled into 11 equally spaced surfaces within the cortical gray matter (Figure 2a). The selected ROIs covered auditory cortex and adjacent areas (Figure 2b, see Figure 1 for all ROIs). The depth profiles of the normalized BOLD response to auditory and visual stimuli are shown for two ROIs in Figure 2c. In the left hemisphere HS ROI, the depth profile in the auditory condition had a concave shape, with the slope of the profile being steepest near the white matter surface. In contrast, in the visual

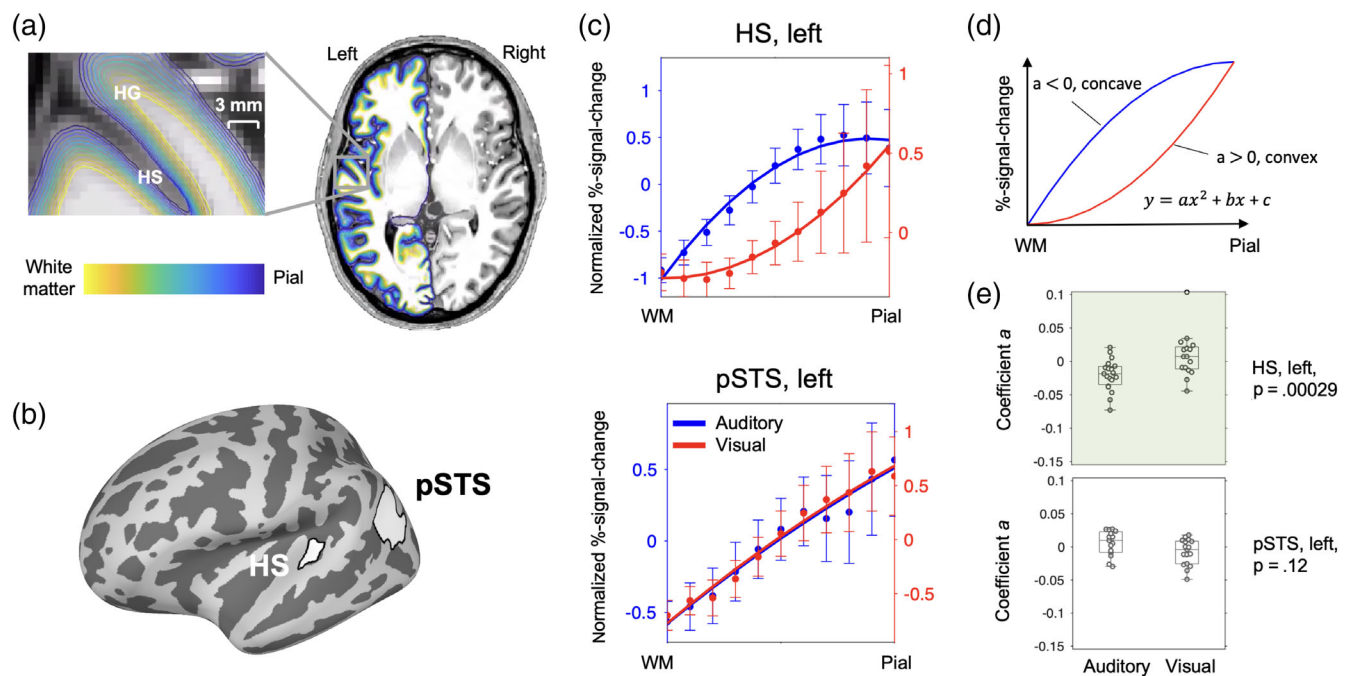


**FIGURE 2** Depth profiles of 7 T fMRI BOLD data. (a) the cortical gray matter was divided into 11 evenly spaced surfaces, shown here superimposed on an anatomical image with 0.75-mm isotropic resolution in a representative subject (yellow: white matter (WM)–gray matter border, blue: pial surface). The enlarged part shows left hemisphere auditory areas including Heschl's gyrus (HG) and sulcus (HS). (b) Two of the regions-of-interest (ROIs) used; an auditory cortex region (HS) and a polymodal area (posterior superior temporal sulcus (pSTS)). The ROIs are illustrated on an inflated left-hemisphere cortical surface. (c) Depth profiles of BOLD %-signal-change for the two ROIs (normalized separately for each condition in each ROI), showing the mean  $\pm$  SEM (13 subjects) on the 11 surfaces in response to auditory (blue dots) and visual (red dots) stimuli. According to the LME model, the depth profiles differed significantly between the auditory and visual conditions in the left HS, but not in the left pSTS. The continuous curves show quadratic regression models fitted to the depth profiles averaged across subjects for visualization of the effect. (d) Interpretation of the coefficient for the quadratic term of the polynomial model: When  $a > 0$  the shape is convex. (e) Results of polynomial fitting to individual subjects. The coefficient  $a$  for the quadratic term in the regression model for individual subjects (dots) in the two ROIs are shown for the auditory and visual stimulation conditions. In HS, the coefficients were significantly different between the conditions (highlighted by green background), being negative for the auditory condition (convex profile) but positive (concave) for visual condition. In pSTS, no significant difference between the auditory and visual conditions was found.

condition the depth profile had a convex shape, with the slope increasing towards the superficial surfaces. In the left pSTS ROI, the depth profiles had a nearly linear shape for both the auditory and the visual condition. The curvilinear shape was characterized by the coefficient  $a$  of the quadratic term in the regression model, such that negative and positive values of  $a$  correspond to concave and convex shapes, respectively (Figure 2d). The values of this coefficient for individual subjects in the two ROIs are shown in Figure 2e. In the auditory cortex ROI (left HS) the mean values differed significantly between the two conditions, being negative (concave shape) in the A condition and positive (convex) in the V condition. In the presumed polymodal area posterior STS, the values were close to zero (linear shape) in both conditions, with no statistically significant differences between them.

### 3.2 | Group analyses of depth profiles

The statistical significance of the parameters of the LME model (Equation 2) are shown in Table S1, and the predicted depth profiles

derived from the values of the LME model are shown in Figures S11a, b. The corresponding results for non-normalized data are shown in Table S2. The LME model for the normalized data indicated a significant *condition* by *surface*<sup>2</sup> interaction, which is of the main interest in this study, in four ROIs: left HG ( $p_{\text{corrected}} = .0014$ ), right HG ( $p_{\text{corrected}} = .00060$ ), left HS ( $p_{\text{corrected}} = .0029$ ), and left pSTG ( $p_{\text{corrected}} = .0014$ ). No significant *condition* by *surface*<sup>2</sup> interactions were found in any of the posterior (polymodal) ROIs.

There were no significant effects for the *intercept*, which is expected for the zero-mean normalized data. In all ROIs, there was a significant main effect of *surface*, reflecting an increase in the response from deep to superficial surfaces. A significant effect of *condition* was found in the left HG, HS, and pSTG, and the right HG. This was somewhat surprising considering that the data for each condition were normalized separately. However, these main effects of *condition* were seen in the same ROIs as the *condition* by *surface*<sup>2</sup> interactions, suggesting that the differences in the nonlinear shape between conditions resulted in an offset of the response levels at the center of the profile ( $x = 0$ ) in the normalized data. Significant *condition* by *surface*

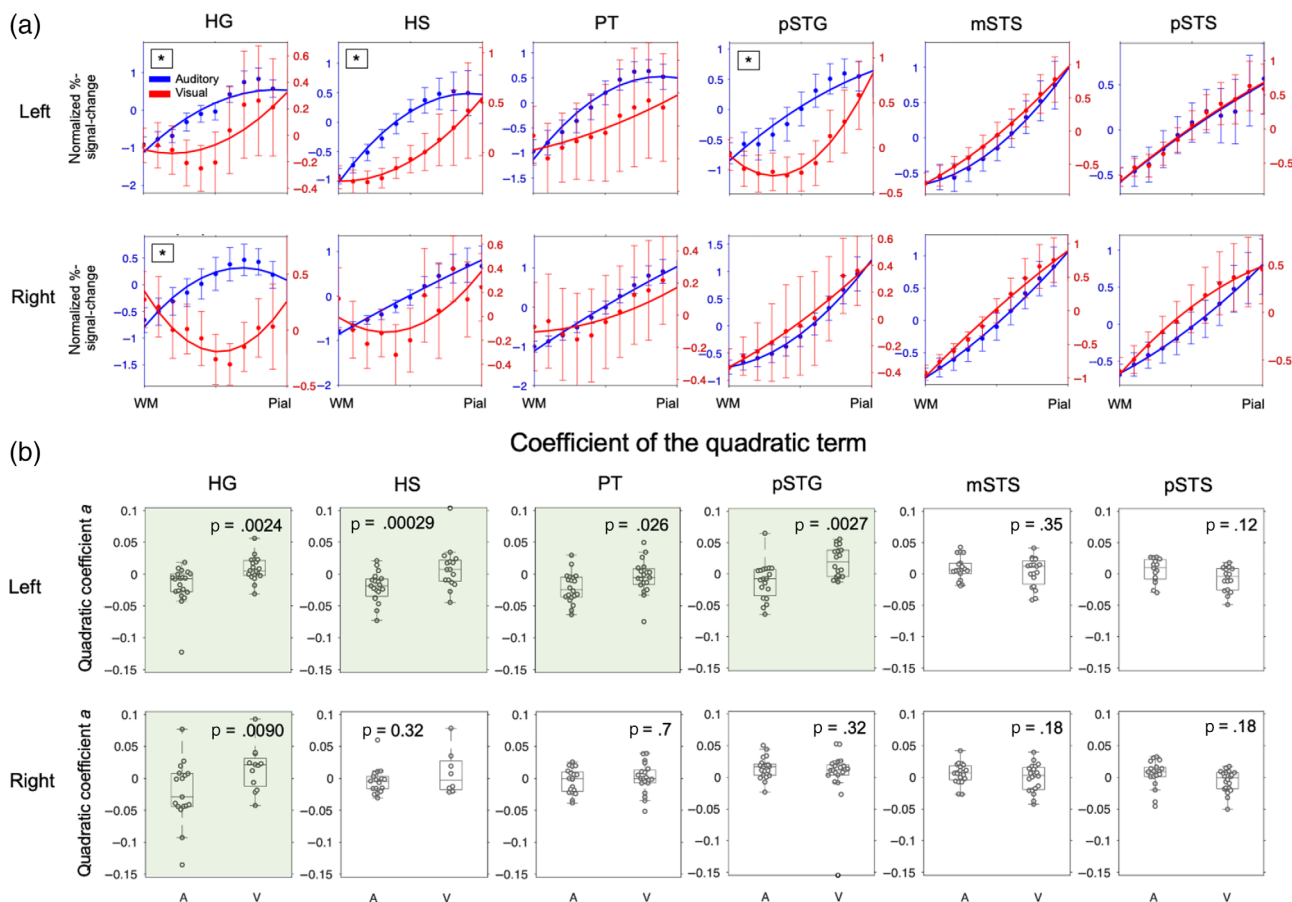


**FIGURE 3** (a) BOLD signal depth profiles for all ROIs. Mean  $\pm$  SEM (13 subjects) %-signal-changes (normalized separately for each condition in each ROI) are shown for the 11 surfaces covering the cortex from the white matter (WM) border to the pial surface for the A (blue dots) and V (red dots) conditions. The continuous curves show quadratic regression models fitted to the depth profiles that were first averaged across the subjects. The data from subjects who had two sessions were averaged across the sessions before calculating the mean and fitting the regression model. Statistical significance ( $p < .05$ ) of condition by surface<sup>2</sup> interaction in the LME model of Equation 2 (see Table S1) is indicated by an asterisk. (b) Coefficients of the quadratic term  $a$  in Equation 1 from a polynomial fit to the normalized BOLD signal depth profiles separately for each subject. The coefficients are shown for all ROIs in the left (top row) and right (bottom) hemisphere for individual subjects (dots). ROIs for which there was a significant difference between the A and V conditions (estimated by the secondary LME model, Equation 4) are highlighted with green background ( $p < .05$ , FDR corrected). The data were normalized separately for each condition in each ROI before fitting the secondary LME model.

interactions were found in the anterior ROIs (HG, HS, PT, pSTG in both hemispheres), presumably reflecting the stronger activation in the A than the V condition, manifested in steeper slopes even after the z-score normalization.

### 3.3 | Polynomial fitting analysis in individual participants

In addition to the statistical analysis using the LME model described above, we further illustrated differences in the depth profile shapes by fitting quadratic regression models to profiles averaged across the subjects (Figure 3a, see Figure S10 for non-normalized data). As a general observation, the shapes of the depth profiles differed more between the A and V conditions in the more anterior ROIs (HG, HS, PT, and pSTG) close to the primary auditory areas, whereas the profiles were similar in the more posterior ROIs (mSTS and pSTS) close to

polymodal areas. Notably, the fitted polynomial curves (Figure 3a) are generally consistent with predicted depth profiles from the LME (Figure S11), showing a similar pattern of concave versus convex shapes in the anterior-posterior axis in the A and V conditions. Furthermore, the results were not sensitive to the selection of voxels within each ROI: the results in Figure 3a, which were based on vertices chosen using the AV condition (Figure S8), were similar to those obtained by using all vertices within each ROI (Figures S11c,d) for averaging the positive response values.

The values of the coefficient for the quadratic term in the polynomial fit ( $a$  in Equation 1) in individual subjects are shown in Figure 3b. This coefficient was significantly different between the conditions ( $A < V$ ) in the left HG, HS, PT, and pSTG, and in the right HG. In all of these ROIs, the mean values of the coefficient were negative (concave shape) in the A condition and positive (convex) in the V condition. Similar differences between the conditions were obtained also with non-normalized data (Figures S13): only one additional ROI (right

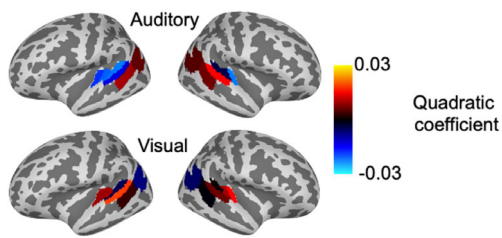


**FIGURE 4** The values of the coefficient for the quadratic term of the polynomial fit ( $a$  in Equation 1), averaged across subjects, shown for all ROIs. Importantly, the progression of the coefficient values from sensory-topomodal regions is reversed between the auditory and visual conditions.

pSTG) showed significant differences (in the opposite direction,  $A > V$ ) for the non-normalized data. The similarity of the results for normalized and non-normalized data suggests that the overall magnitude differences between the A and V conditions had little effect on the results of the analysis of the profile shape as characterized by the quadratic term.

As expected, however, there were several differences between the results for normalized and non-normalized data in the linear and constant terms. The values for all three coefficients  $a$ ,  $b$ , and  $c$  are shown Figures S12 (normalized) and S13 (non-normalized). For the normalized data, significant differences in the coefficient  $b$  for the linear term between the conditions ( $A > V$ ) were seen in the anterior ROIs (bilateral HG, HS, PT, and right pSTG). For the non-normalized data most ROIs (bilateral HG, HS, PT, pSTG, and left mSTS) showed significantly larger values in the A condition for the linear and constant terms; in contrast, the most posterior of our ROIs (bilateral pSTS) showed a significant difference in the opposite direction ( $A < V$ ) in the coefficient for the constant term.

Since the magnitude of the BOLD response differed substantially between the A and V conditions, particularly in the auditory cortex ROIs (see non-normalized data in Figure S10), we further examined whether the observed differences in the shape of the depth profiles were driven by differences in the overall response magnitude. van Dijk et al. (2020) demonstrated that BOLD 3D-EPI amplitude scaled linearly across cortical depths with different response strengths. Thus, when the quadratic coefficients for the A and V conditions have the same sign, an observed difference between them could be simply due to a difference in the overall response magnitude. Importantly, however, Figure 3a shows that the sign (*i.e.*, concavity vs. convexity) was different for A and V conditions in the regions that were statistically significant, and thus those differences in the quadratic coefficients between conditions cannot be explained simply by magnitude differences. Furthermore, we estimated profiles in the A condition using only a subset of vertices such that the average %-signal-changes were, across all depths, closer to those in the V condition. As shown by Figure S14, the shape of the depth profile for A condition for the left HS remained concave. Tables S3 and S4 show LME model results using the subsets of vertices with lower activation levels.

### 3.4 | Cortical surface mapping of depth profile parameters

The mean values of the coefficient for the quadratic term for each ROI are visualized on inflated cortical surfaces in Figure 4, demonstrating a progression pattern of the coefficient values from sensory to polymodal regions that is reversed between A and V conditions.

## 4 | DISCUSSION

The shape of the depth profiles of 1-mm resolution human 7 T fMRI of BOLD signals in response to auditory and visual stimulation differed significantly in ROIs near primary auditory cortices, but not in the adjacent polymodal areas. These results are consistent with previous NHP studies (Lakatos et al., 2007, 2009; Schroeder & Foxe, 2002), and possibly stem from an underlying difference in the laminar distribution of input connections. Near primary auditory regions the slope of the depth profile in the A condition was largest in the deepest surfaces (concave profile), whereas in the V condition the slope was largest near to the superficial surfaces (convex profile). Our results suggest that the shapes of the intracortical BOLD signal profiles could provide a way to differentiate between FF versus FB influences noninvasively in the human brain.

A limited number of previous studies have explicitly focused on the differentiation of FF and FB profiles in the human auditory cortex. One recent fMRI study showed differing depth profiles of attentional and multisensory influences during auditory and/or visual stimulation in human auditory cortex; however, these effects were dominated by deactivations rather than signal increases, and their analysis concentrated on linear and constant shape parameters in two broadly defined ROIs, labeled A1 and PT (Gau et al., 2020). However, the present findings of depth profiles generally increasing toward the pial surface are consistent with results by Chai et al. (2021). In addition to BOLD profiles, Chai et al. measured depth profiles also with VAPER (integrated blood volume and perfusion contrast), which has superior laminar specificity that reduces the draining vein bias towards surface. By combining information by VAPER and BOLD, Chai et al. concluded that auditory stimuli had a mixture of FF and FB effects in anterior PT, whereas visual stimuli had an FB effect in posterior PT; in A1, they only found an FF effect for auditory stimuli. There are some possibilities that might explain the discrepancy between these results and our findings (we found no FB effect for A condition in HG or HS, and we found FB type effect for V condition in HG, HS, and PT), such as selection of the ROIs and voxels, stimuli (their moving vs. our static stimuli) and the general study design. The present study extends the previous findings by comparing curvilinear shapes of BOLD signal depth profiles in auditory vs. nearby polymodal areas.

Our human 7 T fMRI results are in line with regional differences of FF vs. FB influences found in NHPs using measurements of local field potentials (LFP; Lakatos et al., 2007, 2009; Schroeder & Foxe, 2002). Both in nonprimary (Schroeder & Foxe, 2002) and primary (Lakatos et al., 2007, 2009) auditory cortices, auditory responses

have a FF type laminar profile with the earliest activity in the granular middle layer. In contrast, the profiles of cross-sensory visual (and somatosensory) responses resemble those of FB type inputs that arrive predominantly to superficial, and to some degree also to deep layers (Lakatos et al., 2007, 2009; Schroeder & Foxe, 2002). Here, analogously to these LFP studies, the BOLD signal depth profiles to A vs. V stimuli were significantly different in the left HG, HS, pSTG, and right HG ROIs, which encompass primary and some nonprimary areas of the human auditory cortex (Da Costa et al., 2011; Moerel et al., 2014). The concave depth profile observed in the A condition in these areas, with the largest signal relative to a linear shape in the middle part of the profile, could correspond to FF type inputs into the granular layer of the cortex, whereas the convex shape in the V condition could indicate FB type inputs to supra-granular and infra-granular layers. Laminar LFP recordings in NHPs suggest that in polymodal areas, such as the STP, which is located in the superior temporal sulcus in NHP, LFP responses to auditory and visual stimuli both have a FF type laminar profile (Schroeder & Foxe, 2002). This is in line with our present finding of no significant difference between the A and V conditions in the coefficient of the quadratic term of the polynomial fit to the intracortical BOLD profile in the mSTS and pSTS ROIs.

We found the clearest separation between sensory-specific (auditory) and cross-sensory (visual) depth profiles in the left HS. This area may correspond to the lateroposterior region, which is immediately posterior to the primary auditory cortex, as defined in human post-mortem studies (Wallace et al., 2002). This pattern is consistent with previous NHP fMRI studies, which suggest that within the auditory cortex, the effects of cross-sensory stimulation are particularly strong in areas posterior to A1 (Kayser et al., 2009).

The depth profiles in the right pSTG were different from those in its left hemispheric counterparts, as well as in the ROIs of closer to the core of auditory cortex: the right pSTG showed a more convex profile (*i.e.*, more positive quadratic term) in the A than in the V condition. However, values of the quadratic coefficients were small, with nearly linear profiles, resembling the profiles observed for the left and right mSTS. It is also worth noting that the present area pSTG, defined based on the Freesurfer Destrieux atlas, included only the crest of the STG that is near the boundary of higher-order auditory association areas and multisensory cortices, and this area shows much greater individual variability, differing functional connectivity patterns, and more complex feature tuning properties than areas closer to the primary auditory cortex (Moerel et al., 2013; Norman-Haignere et al., 2015; Ren, Hubbard, et al., 2021; Ren, Xu, et al., 2021).

A possible concern for the interpretation of the data is that differences in the overall strength of signals could have confounded the estimation of BOLD depth profiles. Here, we attempted to control for this possibility at the group level, by regressing out the effect of individual variability in baseline amplitude differences between conditions in our LME models. Further, because the amplitude differences were quite large in certain ROIs, we normalized the data to avoid biasing the estimates of the depth profile coefficients in the LME model. However, despite these statistical procedures, we cannot fully exclude the alternative explanation that, due to the underlying neurovascular generation

process, the curvature depends on signal strength. For example, the BOLD signal might start to saturate with high amplitudes of the %-signal-change and thus affect the shape of the depth profile due to a ceiling effect. Thus, as an additional control, we also conducted a more qualitative analysis where we compared the shapes of the depth profiles for A stimuli, which generally triggered much stronger responses in and near auditory cortices than V stimuli. In this analysis, we consecutively iterated the cortical vertices selected to the analysis of A profiles, by excluding vertices where the average %-signal-change across all depths was limited to amplitude of 4 or 2. Although this analysis is limited by the fact that the selected vertices included to the ROI average slightly differed between the estimates, it is interesting to note that the shape of the depth profile for A responses remained similar irrespective of the maximum threshold, consistent with previously reported linear scaling in the visual cortex (van Dijk et al., 2020). However, it is obvious that further studies are still needed to clarify the relationship between the signal strength and the shape of the depth profile.

Another potential limitation to the interpretation of the results is that the BOLD signal depth profiles to cytoarchitecturally defined cortical layers is not straightforward. The thickness of cellular layers varies across the cortex and even across subareas of auditory cortex (Barbas, 2015; Ding et al., 2009; Zachlod et al., 2020). The laminar properties also vary in depth as a function of the curvature of the cortex (Fatterpekar et al., 2003; Hilgetag & Barbas, 2006; Van Essen & Maunsell, 1980), and cortical thickness itself also varies across folding patterns (Fischl & Dale, 2000). Furthermore, even with small voxel size the partial volume effect on the tissue boundaries can contaminate the pure gray matter signal. Some of the nonspecificity of BOLD signal arises from the large draining vessels near the pial surface (Markuerkiaga et al., 2016; Olman et al., 2007; Polimeni et al., 2010; Turner, 2002). Gradient-echo BOLD is most commonly used for fMRI due to its high sensitivity, but the biasing influence of large veins results in a relatively lower specificity. It has been proposed that this bias can be mitigated with spin-echo fMRI, which purportedly suppresses the contribution of large vessels (Duong et al., 2003; Uludag et al., 2009; Yacoub et al., 2003; Zhao et al., 2004). Spin-echo fMRI, however, has much lower overall sensitivity than the present gradient-echo 3D-EPI fMRI method. In addition to BOLD, imaging using sequences such as VASO or VAPER has showed very promising results (see, *e.g.*, Chai et al., 2020; Chai et al., 2021). Future studies using methods that provide better ways for taking the draining vein effect into account (Chai et al., 2021; Heinzle et al., 2016; Markuerkiaga et al., 2016; Marquardt et al., 2018) are thus clearly warranted. Furthermore, combining fMRI with magnetoencephalography or electroencephalography (Bonaiuto, Meyer, et al., 2018; Bonaiuto, Rossiter, et al., 2018) could provide complementary information which would help to interpretate the depth profiles.

## 5 | CONCLUSION

In conclusion, we demonstrated that depth profiles for sensory-specific auditory and cross-sensory visual activity were distinct in



auditory regions but similar in polymodal regions in human BOLD signals. These findings suggest that FF vs. FB type influences could be distinguished from one another with cortical depth analyses of high-resolution fMRI, thus opening new perspectives in investigating detailed hierarchical organization between cortical regions in humans. Further experimental studies are still needed to clarify how the overall signal strength influences BOLD depth profiles of intramodal FF and cross-sensory FB type responses.

#### DATA AVAILABILITY STATEMENT

The data and code for reproducing the main findings of the paper are available on <http://github.com/klankinen/7T-feedforward-feedback>. The data of this study are available from the corresponding author upon reasonable request.

#### ORCID

Kaisu Lankinen  <https://orcid.org/0000-0003-2210-2385>

Seppo P. Ahlfors  <https://orcid.org/0000-0001-7674-6931>

Fahimeh Mamashli  <https://orcid.org/0000-0002-7024-943X>

Tommi Raji  <https://orcid.org/0000-0001-7439-7491>

Jonathan R. Polimeni  <https://orcid.org/0000-0002-1348-1179>

Jyrki Ahveninen  <https://orcid.org/0000-0001-9058-8669>

#### REFERENCES

- Ahveninen, J., Chang, W. T., Huang, S., Keil, B., Kopco, N., Rossi, S., Bonmassar, G., Witzel, T., & Polimeni, J. R. (2016). Intracortical depth analyses of frequency-sensitive regions of human auditory cortex using 7TfMRI. *NeuroImage*, *143*, 116–127.
- Barbas, H. (2015). General cortical and special prefrontal connections: Principles from structure to function. *Annual Review of Neuroscience*, *38*, 269–289.
- Beauchamp, M. S., Lee, K. E., Argall, B. D., & Martin, A. (2004). Integration of auditory and visual information about objects in superior temporal sulcus. *Neuron*, *41*, 809–823.
- Blazewaska, A. I., Fischl, B., Wald, L. L., & Polimeni, J. R. (2019). Intracortical smoothing of small-voxel fMRI data can provide increased detection power without spatial resolution losses compared to conventional large-voxel fMRI data. *NeuroImage*, *189*, 601–614.
- Bonaiuto, J. J., Meyer, S. S., Little, S., Rossiter, H., Callaghan, M. F., Dick, F., Barnes, G. R., & Bestmann, S. (2018). Lamina-specific cortical dynamics in human visual and sensorimotor cortices. *eLife*, *7*, e33977.
- Bonaiuto, J. J., Rossiter, H. E., Meyer, S. S., Adams, N., Little, S., Callaghan, M. F., Dick, F., Bestmann, S., & Barnes, G. R. (2018). Non-invasive laminar inference with MEG: Comparison of methods and source inversion algorithms. *NeuroImage*, *167*, 372–383.
- Chai, Y., Li, L., Huber, L., Poser, B. A., & Bandettini, P. A. (2020). Integrated VASO and perfusion contrast: A new tool for laminar functional MRI. *NeuroImage*, *207*, 116358.
- Chai, Y., Liu, T. T., Marrett, S., Li, L., Khojandi, A., Handwerker, D. A., Alink, A., Muckli, L., & Bandettini, P. A. (2021). Topographical and laminar distribution of audiovisual processing within human planum temporale. *Progress in Neurobiology*, *205*, 102121.
- Da Costa, S., van der Zwaag, W., Marques, J. P., Frackowiak, R. S., Clarke, S., & Saenz, M. (2011). Human primary auditory cortex follows the shape of Heschl's gyrus. *The Journal of Neuroscience*, *31*, 14067–14075.
- De Martino, F., Moerel, M., Ugurbil, K., Goebel, R., Yacoub, E., & Formisano, E. (2015). Frequency preference and attention effects across cortical depths in the human primary auditory cortex. *Proceedings of the National Academy of Sciences of the United States of America*, *112*, 16036–16041.
- Desikan, R. S., Segonne, F., Fischl, B., Quinn, B. T., Dickerson, B. C., Blacker, D., Buckner, R. L., Dale, A. M., Maguire, R. P., Hyman, B. T., Albert, M. S., & Killiany, R. J. (2006). An automated labeling system for subdividing the human cerebral cortex on MRI scans into gyral based regions of interest. *NeuroImage*, *31*, 968–980.
- Ding, S. L., Van Hoesen, G. W., Cassell, M. D., & Poremba, A. (2009). Parcellation of human temporal polar cortex: A combined analysis of multiple cytoarchitectonic, chemoarchitectonic, and pathological markers. *The Journal of Comparative Neurology*, *514*, 595–623.
- Duong, T. Q., Yacoub, E., Adriany, G., Hu, X., Ugurbil, K., & Kim, S. G. (2003). Microvascular BOLD contribution at 4 and 7 T in the human brain: Gradient-echo and spin-echo fMRI with suppression of blood effects. *Magnetic Resonance in Medicine*, *49*, 1019–1027.
- Fatterpekar, G. M., Delman, B. N., Boonn, W. W., Gultekin, S. H., Fayad, Z. A., Hoff, P. R., & Naidich, T. P. (2003). MR microscopy of normal human brain. *Magnetic Resonance Imaging Clinics of North America*, *11*, 641–653.
- Felleman, D. J., & Van Essen, D. C. (1991). Distributed hierarchical processing in the primate cerebral cortex. *Cerebral Cortex*, *1*, 1–47.
- Finn, E. S., Huber, L., Jangraw, D. C., Molfese, P. J., & Bandettini, P. A. (2019). Layer-dependent activity in human prefrontal cortex during working memory. *Nature Neuroscience*, *22*, 1687–1695.
- Fischl, B. (2012). FreeSurfer. *NeuroImage*, *62*, 774–781.
- Fischl, B., & Dale, A. M. (2000). Measuring the thickness of the human cerebral cortex from magnetic resonance images. *Proceedings of the National Academy of Sciences of the United States of America*, *97*, 11050–11055.
- Fischl, B., van der Kouwe, A., Destrieux, C., Halgren, E., Segonne, F., Salat, D. H., Busa, E., Seidman, L. J., Goldstein, J., Kennedy, D., Caviness, V., Makris, N., Rosen, B., & Dale, A. M. (2004). Automatically parcellating the human cerebral cortex. *Cerebral Cortex*, *14*, 11–22.
- Foxe, J. J., & Schroeder, C. E. (2005). The case for feedforward multisensory convergence during early cortical processing. *Neuroreport*, *16*, 419–423.
- Foxe, J. J., Wylie, G. R., Martinez, A., Schroeder, C. E., Javitt, D. C., Guilfoyle, D., Ritter, W., & Murray, M. M. (2002). Auditory-somatosensory multisensory processing in auditory association cortex: An fMRI study. *Journal of Neurophysiology*, *88*, 540–543.
- Fracasso, A., Luijten, P. R., Dumoulin, S. O., & Petridou, N. (2018). Laminar imaging of positive and negative BOLD in human visual cortex at 7T. *NeuroImage*, *164*, 100–111.
- Gau, R., Bazin, P. L., Trampel, R., Turner, R., & Noppeney, U. (2020). Resolving multisensory and attentional influences across cortical depth in sensory cortices. *eLife*, *9*, e46856.
- Ghazanfar, A. A., & Schroeder, C. E. (2006). Is neocortex essentially multisensory? *Trends in Cognitive Sciences*, *10*, 278–285.
- Greve, D. N., & Fischl, B. (2009). Accurate and robust brain image alignment using boundary-based registration. *NeuroImage*, *48*, 63–72.
- Griswold, M. A., Jakob, P. M., Heidemann, R. M., Nittka, M., Jellus, V., Wang, J., Kiefer, B., & Haase, A. (2002). Generalized autocalibrating partially parallel acquisitions (GRAPPA). *Magnetic Resonance in Medicine*, *47*, 1202–1210.
- Heinze, J., Koopmans, P. J., den Ouden, H. E. M., Raman, S., & Stephan, K. E. (2016). A hemodynamic model for layered BOLD signals. *NeuroImage*, *125*, 556–570.
- Hilgetag, C. C., & Barbas, H. (2006). Role of mechanical factors in the morphology of the primate cerebral cortex. *PLoS Computational Biology*, *2*, e22.
- Huber, L., Tse, D. H. Y., Wiggins, C. J., Uludag, K., Kashyap, S., Jangraw, D. C., Bandettini, P. A., Poser, B. A., & Ivanov, D. (2018). Ultra-high resolution blood volume fMRI and BOLD fMRI in humans at 9.4T: Capabilities and challenges. *NeuroImage*, *178*, 769–779.
- Kayser, C., & Logothetis, N. K. (2007). Do early sensory cortices integrate cross-modal information? *Brain Structure & Function*, *212*, 121–132.

- Kayser, C., Petkov, C. I., Augath, M., & Logothetis, N. K. (2005). Integration of touch and sound in auditory cortex. *Neuron*, *48*, 373–384.
- Kayser, C., Petkov, C. I., & Logothetis, N. K. (2009). Multisensory interactions in primate auditory cortex: fMRI and electrophysiology. *Hearing Research*, *258*, 80–88.
- Keil, B., Triantafyllou, C., Hamm, M., & Wald, L. L. (2010). Design optimization of a 32-channel head coil at 7T. *Proceedings of the International Society for Magnetic Resonance in Medicine*, *18*, 1493.
- Klein, B. P., Fracasso, A., van Dijk, J. A., Paffen, C. L. E., Te Pas, S. F., & Dumoulin, S. O. (2018). Cortical depth dependent population receptive field attraction by spatial attention in human V1. *NeuroImage*, *176*, 301–312.
- Kok, P., Bains, L. J., van Mourik, T., Norris, D. G., & de Lange, F. P. (2016). Selective activation of the deep layers of the human primary visual cortex by top-down feedback. *Current Biology*, *26*, 371–376.
- Lakatos, P., Chen, C. M., O'Connell, M. N., Mills, A., & Schroeder, C. E. (2007). Neuronal oscillations and multisensory interaction in primary auditory cortex. *Neuron*, *53*, 279–292.
- Lakatos, P., O'Connell, M. N., Barczak, A., Mills, A., Javitt, D. C., & Schroeder, C. E. (2009). The leading sense: Supramodal control of neurophysiological context by attention. *Neuron*, *64*, 419–430.
- Lawrence, S. J., Norris, D. G., & de Lange, F. P. (2019). Dissociable laminar profiles of concurrent bottom-up and top-down modulation in the human visual cortex. *eLife*, *8*, e44422.
- Markuerkiaga, I., Barth, M., & Norris, D. G. (2016). A cortical vascular model for examining the specificity of the laminar BOLD signal. *NeuroImage*, *132*, 491–498.
- Marquardt, I., Schneider, M., Gulban, O. F., Ivanov, D., & Uludag, K. (2018). Cortical depth profiles of luminance contrast responses in human V1 and V2 using 7 T fMRI. *Human Brain Mapping*, *39*, 2812–2827.
- Moerel, M., De Martino, F., & Formisano, E. (2014). An anatomical and functional topography of human auditory cortical areas. *Frontiers in Neuroscience*, *8*, 225.
- Moerel, M., De Martino, F., Santoro, R., Ugurbil, K., Goebel, R., Yacoub, E., & Formisano, E. (2013). Processing of natural sounds: Characterization of multipeak spectral tuning in human auditory cortex. *The Journal of Neuroscience*, *33*, 11888–11898.
- Moerel, M., De Martino, F., Ugurbil, K., Formisano, E., & Yacoub, E. (2018). Evaluating the columnar stability of acoustic processing in the human auditory cortex. *The Journal of Neuroscience*, *38*, 7822–7832.
- Moerel, M., De Martino, F., Ugurbil, K., Yacoub, E., & Formisano, E. (2019). Processing complexity increases in superficial layers of human primary auditory cortex. *Scientific Reports*, *9*, 5502.
- Muckli, L., De Martino, F., Vizioli, L., Petro, L. S., Smith, F. W., Ugurbil, K., Goebel, R., & Yacoub, E. (2015). Contextual feedback to superficial layers of V1. *Current Biology*, *25*, 2690–2695.
- Noesselt, T., Rieger, J. W., Schoenfeld, M. A., Kanowski, M., Hinrichs, H., Heinze, H. J., & Driver, J. (2007). Audiovisual temporal correspondence modulates human multisensory superior temporal sulcus plus primary sensory cortices. *The Journal of Neuroscience*, *27*, 11431–11441.
- Norman-Haignere, S., Kanwisher, N. G., & McDermott, J. H. (2015). Distinct cortical pathways for music and speech revealed by hypothesis-free voxel decomposition. *Neuron*, *88*, 1281–1296.
- Norris, D. G., & Polimeni, J. R. (2019). Laminar (f)MRI: A short history and future prospects. *NeuroImage*, *197*, 643–649.
- Olman, C. A., Inati, S., & Heeger, D. J. (2007). The effect of large veins on spatial localization with GE BOLD at 3 T: Displacement, not blurring. *NeuroImage*, *34*, 1126–1135.
- Petro, L. S., & Muckli, L. (2017). The laminar integration of sensory inputs with feedback signals in human cortex. *Brain and Cognition*, *112*, 54–57.
- Polimeni, J. R., Fischl, B., Greve, D. N., & Wald, L. L. (2010). Laminar analysis of 7T BOLD using an imposed spatial activation pattern in human V1. *NeuroImage*, *52*, 1334–1346.
- Polimeni, J. R., Renvall, V., Zaretskaya, N., & Fischl, B. (2018). Analysis strategies for high-resolution UHF-fMRI data. *NeuroImage*, *168*, 296–320.
- Poser, B. A., Koopmans, P. J., Witzel, T., Wald, L. L., & Barth, M. (2010). Three dimensional echo-planar imaging at 7 tesla. *NeuroImage*, *51*, 261–266.
- Raij, T., Ahveninen, J., Lin, F. H., Witzel, T., Jääskeläinen, I. P., Letham, B., Israeli, E., Sahyoun, C., Vasios, C., Stufflebeam, S., Hämäläinen, M., & Belliveau, J. W. (2010). Onset timing of cross-sensory activations and multisensory interactions in auditory and visual sensory cortices. *The European Journal of Neuroscience*, *31*, 1772–1782.
- Raij, T., Uutela, K., & Hari, R. (2000). Audiovisual integration of letters in the human brain. *Neuron*, *28*, 617–625.
- Ren, J., Hubbard, C. S., Ahveninen, J., Cui, W., Li, M., Peng, X., Luan, G., Han, Y., Li, Y., Shinn, A. K., Wang, D., Li, L., & Liu, H. (2021). Dissociable auditory Cortico-cerebellar pathways in the human brain estimated by intrinsic functional connectivity. *Cerebral Cortex*, *31*, 2898–2912.
- Ren, J., Xu, T., Wang, D., Li, M., Lin, Y., Schoeppe, F., Ramirez, J. S. B., Han, Y., Luan, G., Li, L., Liu, H., & Ahveninen, J. (2021). Individual variability in functional Organization of the Human and Monkey Auditory Cortex. *Cerebral Cortex*, *31*, 2450–2465.
- Rockland, K. S., & Pandya, D. N. (1979). Laminar origins and terminations of cortical connections of the occipital lobe in the rhesus monkey. *Brain Research*, *179*, 3–20.
- Rohe, T., & Noppeney, U. (2016). Distinct computational principles govern multisensory integration in primary sensory and association cortices. *Current Biology*, *26*, 509–514.
- Schroeder, C. E., & Foxe, J. (2005). Multisensory contributions to low-level, 'unisensory' processing. *Current Opinion in Neurobiology*, *15*, 454–458.
- Schroeder, C. E., & Foxe, J. J. (2002). The timing and laminar profile of converging inputs to multisensory areas of the macaque neocortex. *Brain Research. Cognitive Brain Research*, *14*, 187–198.
- Schroeder, C. E., Lindsley, R. W., Specht, C., Marcovici, A., Smiley, J. F., & Javitt, D. C. (2001). Somatosensory input to auditory association cortex in the macaque monkey. *Journal of Neurophysiology*, *85*, 1322–1327.
- Turner, R. (2002). How much cortex can a vein drain? Downstream dilution of activation-related cerebral blood oxygenation changes. *NeuroImage*, *16*, 1062–1067.
- Uludag, K., Muller-Bierl, B., & Ugurbil, K. (2009). An integrative model for neuronal activity-induced signal changes for gradient and spin echo functional imaging. *NeuroImage*, *48*, 150–165.
- van der Kouwe, A. J., Benner, T., Salat, D. H., & Fischl, B. (2008). Brain morphometry with multiecho MPRAGE. *NeuroImage*, *40*, 559–569.
- van Dijk, J. A., Fracasso, A., Petridou, N., & Dumoulin, S. O. (2020). Linear systems analysis for laminar fMRI: Evaluating BOLD amplitude scaling for luminance contrast manipulations. *Scientific Reports*, *10*, 5462.
- van Dijk, J. A., Fracasso, A., Petridou, N., & Dumoulin, S. O. (2021). Validating linear systems analysis for laminar fMRI: Temporal additivity for stimulus duration manipulations. *Brain Topography*, *34*, 88–101.
- Van Essen, D. C., & Maunsell, J. H. (1980). Two-dimensional maps of the cerebral cortex. *The Journal of Comparative Neurology*, *191*, 255–281.
- Walker, G. M., & Hickok, G. (2016). Bridging computational approaches to speech production: The semantic-lexical-auditory-motor model (SLAM). *Psychonomic Bulletin & Review*, *23*, 339–352.
- Wallace, M. N., Johnston, P. W., & Palmer, A. R. (2002). Histochemical identification of cortical areas in the auditory region of the human brain. *Experimental Brain Research*, *143*, 499–508.
- Wilkinson, G. N., & Rogers, C. E. (1973). Symbolic description of factorial models for analysis of variance. *Journal of the Royal Statistical Society*, *22*, 392–399.
- Wu, P. Y., Chu, Y. H., Lin, J. L., Kuo, W. J., & Lin, F. H. (2018). Feature-dependent intrinsic functional connectivity across cortical depths in the human auditory cortex. *Scientific Reports*, *8*, 13287.
- Yacoub, E., Duong, T. Q., Van De Moortele, P. F., Lindquist, M., Adriany, G., Kim, S. G., Ugurbil, K., & Hu, X. (2003). Spin-echo fMRI in humans using high spatial resolutions and high magnetic fields. *Magnetic Resonance in Medicine*, *49*, 655–664.

- Yang, J., Huber, L., Yu, Y., & Bandettini, P. A. (2021). Linking cortical circuit models to human cognition with laminar fMRI. *Neuroscience and Biobehavioral Reviews*, *128*, 467–478.
- Zachlod, D., Ruttgers, B., Bludau, S., Mohlberg, H., Langner, R., Zilles, K., & Amunts, K. (2020). Four new cytoarchitectonic areas surrounding the primary and early auditory cortex in human brains. *Cortex*, *128*, 1–21.
- Zaretskaya, N., Fischl, B., Reuter, M., Renvall, V., & Polimeni, J. R. (2015). Characterization of cortical surface reconstruction for sub-millimeter 7T MPRAGE using FreeSurfer. *Annual Meeting of the Organization for Human Brain Mapping*, *21*, 4029.
- Zeki, S. (2018). The rough seas of cortical cartography. *Trends in Neurosciences*, *41*, 242–244.
- Zhao, F., Wang, P., & Kim, S. G. (2004). Cortical depth-dependent gradient-echo and spin-echo BOLD fMRI at 9.4T. *Magnetic Resonance in Medicine*, *51*, 518–524.

## SUPPORTING INFORMATION

Additional supporting information can be found online in the Supporting Information section at the end of this article.

**How to cite this article:** Lankinen, K., Ahlfors, S. P., Mamashli, F., Blazejewska, A. I., Raij, T., Turpin, T., Polimeni, J. R., & Ahveninen, J. (2023). Cortical depth profiles of auditory and visual 7 T functional MRI responses in human superior temporal areas. *Human Brain Mapping*, *44*(2), 362–372. <https://doi.org/10.1002/hbm.26046>